0.1 Drag force experiments

As we introduced in the last section of **Experimental approach** chapter, we used the full frequency sweep method for vibrating wire and tuning fork. Each point on following graphs was obtained by a pair of full frequency sweeps across the resonance of given oscillator. One sweep was performed with increasing frequency and the second one with decreasing frequency, which made us confident that no hysteresis effect was present.

We present all the measurements in the form of typical hydrodynamic visualizations (velocity-force response, drag coefficients and appropriate dimensionless numbers) of oscillating wire, torsional disc and tuning fork, respectively.

0.1.1 Vibrating wire

We were measuring the voltage in phase with the driving current to obtain the resonant response. Above high enough applied drives ($\sim 0.8\,\mathrm{mA}$ at temperature $1.67\,\mathrm{K}$ responding in $\sim 0.1\,\mathrm{m/s}$ peak velocity), there was present a frequency shift and a *peak softening* effect. Together with a poor calibration of magnetic field produced by permanent magnets, the peak velocity on the wire top is known with the accuracy about $\pm 20\%$. Fortunately, this error doesn't affect the scaling process.

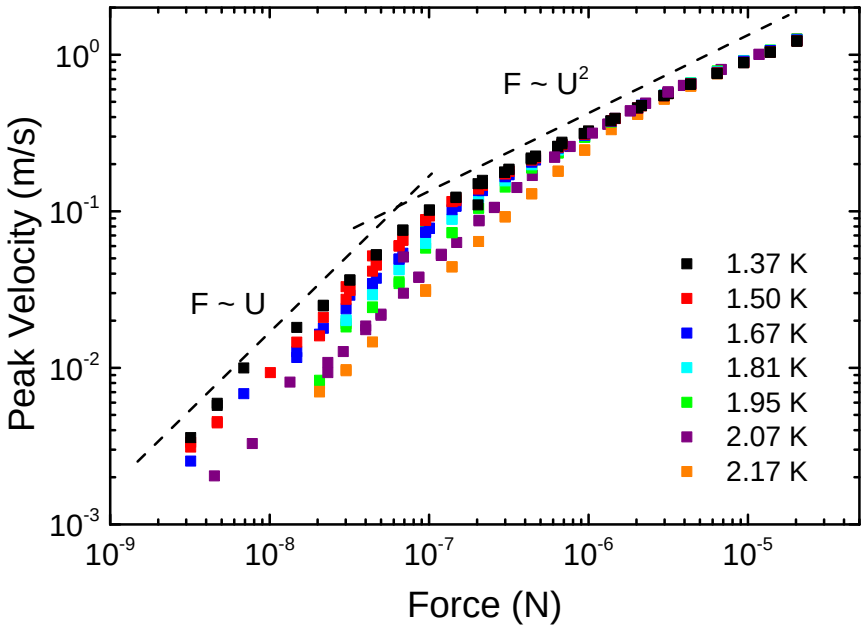

Figure 1: Plot of peak velocity U_0 against the applied peak force F_0 for the vibrating wire submerged in superfluid ^{4}He at several temperatures. The black dashed lines serve as sketch of theoretical laminar and turbulent regimes.

We plotted in **Figure (1)** the peak velocity of the wire top U_0 against the applied peak force F_0 at various temperatures from two-fluid regime ($T > 1.0\,\mathrm{K}$).

Clearly, the wire exhibits linear drag at low velocities and non-linear additional drag in the area of higher velocities. The energy losses of the wire in the low-velocity part are dominated by the viscous drag of the present normal component. Other loss mechanisms like acoustic emission are in principle present as well, but neglected in further discussion. The additional dissipation process in the higher-velocity part indicates either classical or quantum turbulence (or both) and the measured drag F_0 is roughly proportional to U_0^2.

Next we plotted in **Figure (2)** the classical drag coefficient as a function of peak force and velocity $C_D \sim F_0/U_0^2$ using the same data as presented in **Figure (1)**.

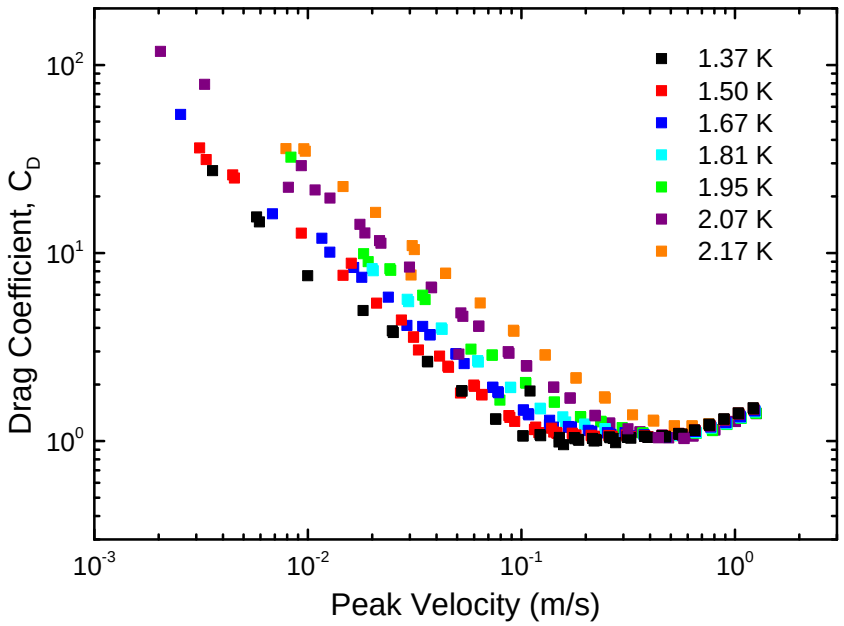

Figure 2: Plot of drag coefficient C_D against the velocity peak response U_0 for the vibrating wire at several temperatures.

In order to perform the universal scaling, we collapse the contribution of the normal component in the following way:

$$C_D^n \leftarrow C_D \frac{\rho}{\rho_n}\,, \qquad \mathrm{Dn} \leftarrow U_0 \sqrt{\frac{2\rho_n}{\eta\omega}}\,, \tag{1}$$

where η is the dynamical viscosity of Helium-II for a given temperature. Relations in (1) are applied in the same way as described (**??**), (**??**) in the last section of **Theoretical background** chapter.
The resulting plot **Figure (3)** clearly collapses all the linear parts of the measured

drag. However, the theoretical pre-factor ($\Phi_{\rm cyl} = 4\pi$) is smaller than the fitted one ($\Phi \sim 26$). This is most likely caused by the irregularities on the surface of the wire. Indeed, excrescences of order 5μm were observed on the 40μm wire under an optical microscope.

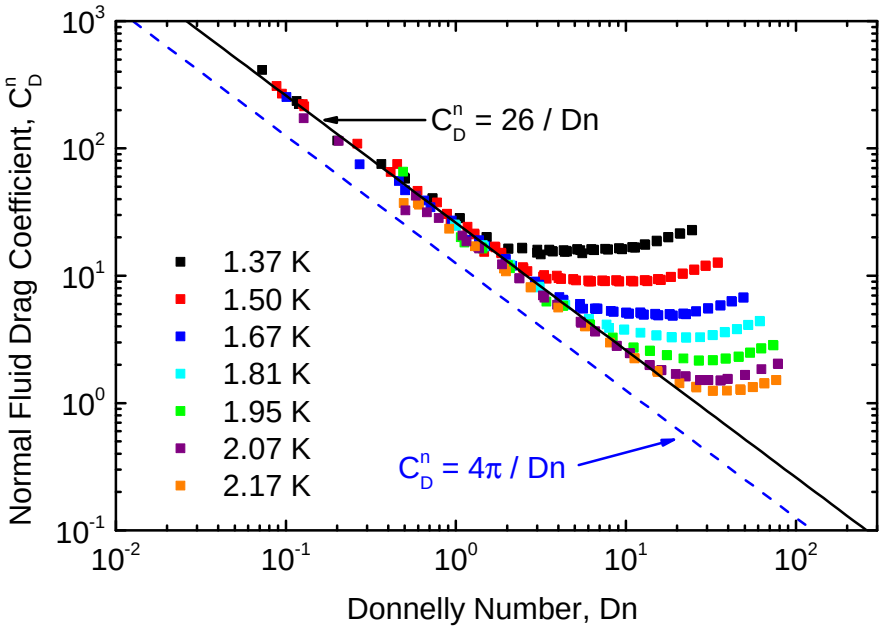

Figure 3: Plot of normal fluid drag coefficient C_D^n against the dimensionless Donnelly number (Dn) for the vibrating wire at several temperatures.The blue dashed line shows the expected theoretical dependence [**?**] for a smooth cylinder. The solid black line is a numerical fit of the linear part of data.

One may see from the **Figure (3)** that all temperature curves are visually sorted ascendingly as the non-linear behaviour occurs at some starting points. This is clear sign the Donnelly number cannot govern the turbulent process and thus it is a clear sign of the onset of quantum turbulence by the superfluid component.

0.1.2 Oscillating disc

The (torsionally) oscillating disc differs from the vibrating wire in several technicalities:

- Oscillating disc does not displace any fluid and thus The superfluid is at rest unless quantized vorticity is produced
- It is not possible to perform measurements in a steady state of flow, but decayed flow was measured instead
- Drag force has to be inferred from the decaying amplitude of oscillator deflection.

As a consequence of mentioned differences (examples showed in **Figure 4**), we have to substitute $U_0 = \omega R \phi_0$ within the Donnelly number and define a new drag coefficient, specific for our mechanical system of torsionally oscillating disc in a viscous fluid of density ρ_n as:

$$C_D^n \leftarrow \frac{2M_f}{A\rho_n \Omega_0^2 R^3}\,, \qquad \mathrm{Dn} \leftarrow R\omega\phi_0 \sqrt{\frac{2\rho_n}{\eta\omega}}\,, \tag{2}$$

where M_f is the moment of friction forces, R the radius of the disc, $A = \pi R^2$ the area of the disc and Ω_0 is the amplitude of angular frequency $\omega(t)$. It was already showed [**?**] the relation between such drag coefficient (2) can be expressed in laminar flow in terms of the Donnelly number as $C_D^n = \Phi/\mathrm{Dn}$ with the pre-factor $\Phi_{\mathrm{disc}} = 2$.

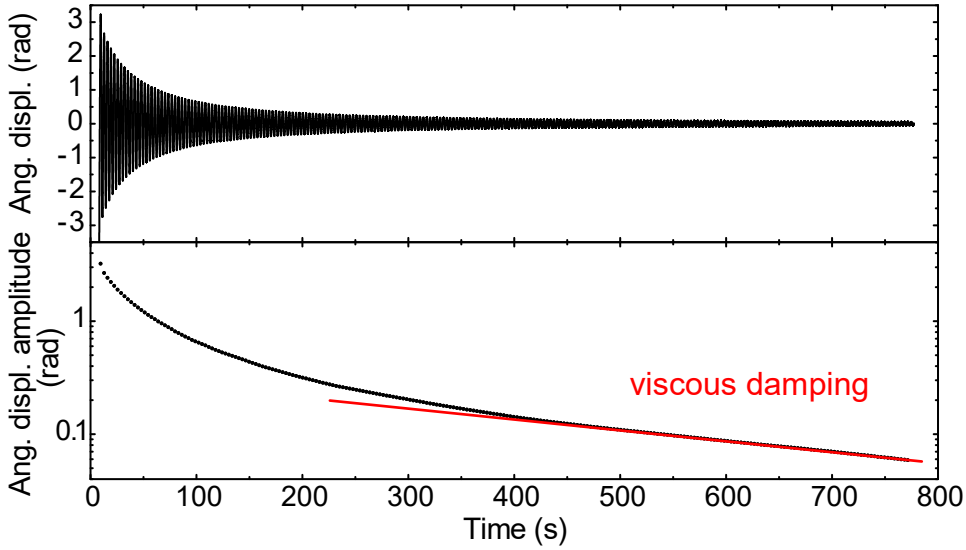

Figure 4: Example of angular displacement measurement in time of the torsionally oscillating disc. Top picture: The decreasing angular displacement amplitudes $\phi_0(t)$. Bottom picture: The logarithmic plot $\phi_0(t)$ shows two distinct regions – nonlinear decay in the area of earlier times $t < 400$ due to turbulent drag forces and an exponential (viscous) decay due to laminar flow of the normal component at the later times $t > 500$.

We plot the re-defined drag coefficient (2) against the Donnelly number in **Figure 5**.

Again, as in case of vibratig wire, in the area of small values of Donnelly number, the data clearly collapse to a single dependence, which illustrates the universal scaling idea. One would naturally expect the normal component to transit to turbulent regime earlier than the superfluid one since the oscillating disc directly moves only with the normal component. However, **Figure 5** clearly shows that non-linearities are not characterized by a single value of Dn, but rather continuously with ascending temperature. This implies that instabilities cannot be explained by pure viscous fluid dynamics and must relate to

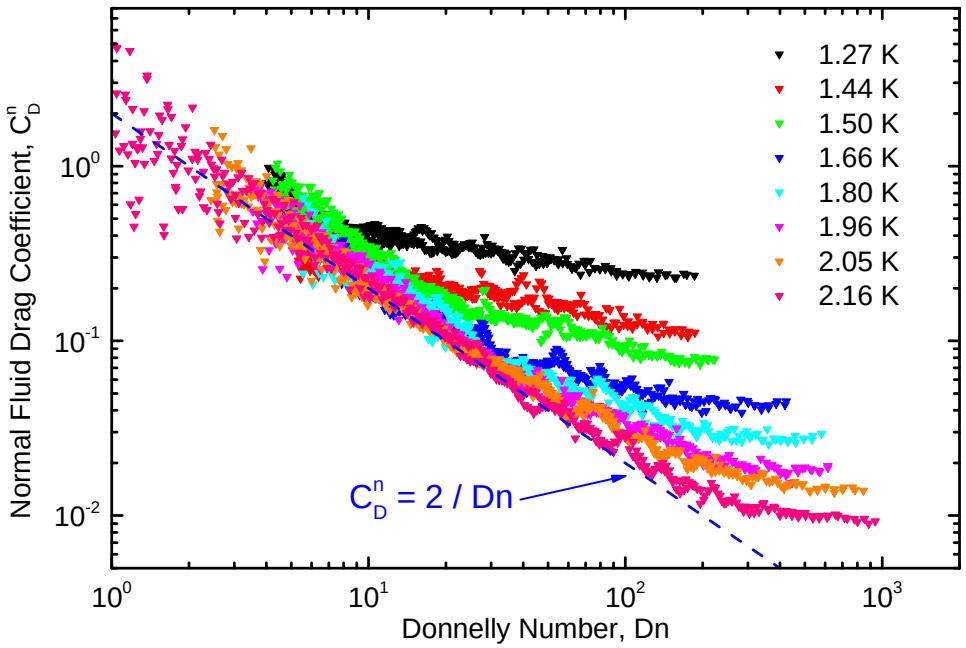

Figure 5: Plot of re-defined fluid drag coefficient C_D^n against the dimensionless Donnelly number (Dn) for the torsionally oscillating disc at several temperatures.
The blue dashed line shows the expected theoretical dependence [**?**] for viscous drag. The temperature-dependent and temperature-ascending starting points of non-linearities are a clear sign of the onset of quantum turbulence by the superfluid component.

the quantum turbulence of vortex tangle.

0.1.3 Tuning fork

In case of used quartz tuning fork (with described geometry and resonant specifics from **Experimental approach**), the resonant response was experimentally measured in the same way as was with vibrating wire - by an analysing of in-phase current response. Electrical quantities are then converted into physical attributes according to relations **??**, which are dependent on fork constants a_{f0}, a_{f1} for the fundamental and overtone mode, respectively. In order to measure them, we had to perform a series of frequency sweeps in low-temperature vacuum.
We estimate the uncertainty of fork constants to be of 10% since velocity calculation errors was proven using optical experiments.

We plot in **Figure 6** the peak velocity U_0 of the top of fork prong, against the applied force F_0 at various temperatures from two-fluid regime ($T > 1.0\,\mathrm{K}$). Also, we plot in **Figure 7** the classical drag coefficient C_D against the peak velocity U_0. Both plots are visualised for paired fundamental and overtone modes.

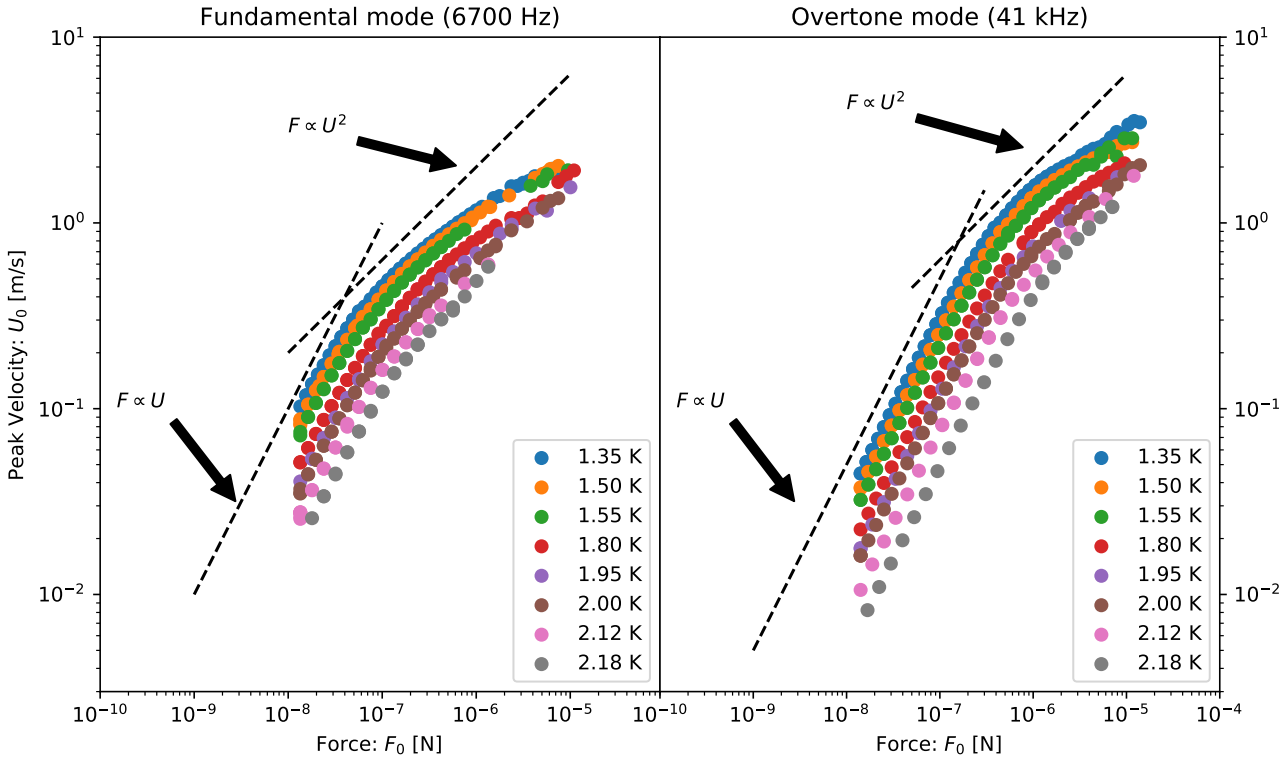

Figure 6: Plot of peak velocity U_0 against the applied peak force F_0 for the oscillating tuning fork submerged in superfluid ^{4}He at several temperatures.
Left image: Measurements in fork's fundamental mode, Right image: Measurements in fork's overtone mode, Black dashed lines serve as a sketch of theoretical laminar and turbulent regimes.

As expected, the tuning fork exhibits a linear drag in the area of low velocities regardless on the temperature from the studied range. Then, approximately above 0.1 m/s an increased drag was observed and some of some curves below certain temperature seem to be independent and thus share the value for critical velocity.

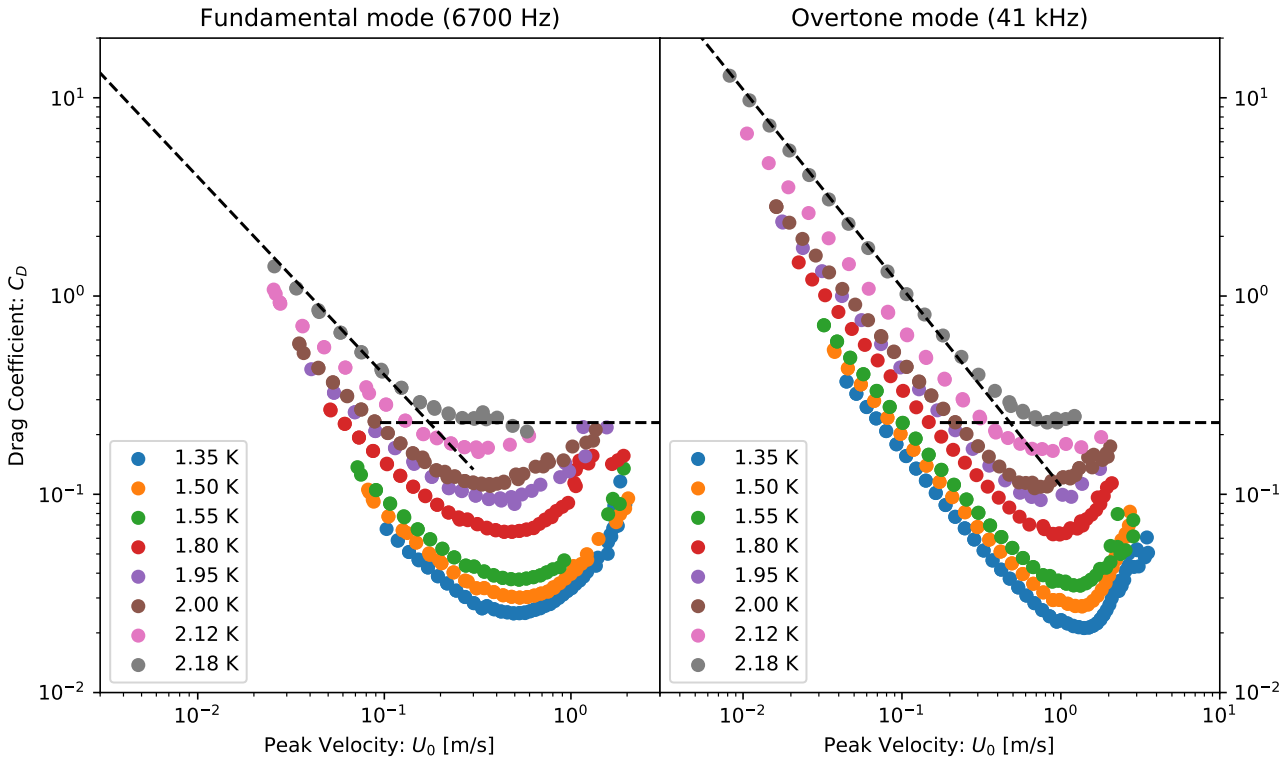

Figure 7: Plot of drag coefficient C_D against the velocity peak response U_0 for the oscillating tuning fork submerged in superfluid ^{4}He at several temperatures.
Left image: Measurements in fork's fundamental mode, Right image: Measurements in fork's overtone mode, Black dashed lines serve as a sketch of theoretical laminar and turbulent regimes.

Again, to characterize the normal component flow, we plot in **Figure 8** the normal drag coefficient against the dimensionless Donnelly number for both resonant modes. The calculations were done as we stated in (1).

With no doubt, in the area of low Donnelly values, the dependencies collapse to a single dependence representing the laminar regime with the shared pre-factor $\Phi = 4.9$. In contrast to the results obtained with the vibrating wire or oscillating disc, we recognize a critical value of Donnelly number $\mathrm{Dn}_{\mathrm{crit}}$ above which certain group of temperatures (above $T \sim 1.6\,\mathrm{K}$) curves non-linearly deviate. The onset of turbulence is governed by a single Donnelly number value $\mathrm{Dn}_{\mathrm{crit}} \sim 12$ and thus dominated by the normal component of Helium-II.

Temperature curves $T \in \{1.35\,\mathrm{K}, 1.50\,\mathrm{K}, 1.55\,\mathrm{K}\}$ shows the nonlinearity onset in the same way as we observed in the case of vibrating wire or the oscillation disc - turbulence originating at various Donnelly numbers, thus rather governed by a single critical velocity value U_{crit}.

We note that it is interesting to find the critical Donnelly number and laminar pre-factor $\Phi = 4.9$ to be same for both oscillation modes. The shared critical $\mathrm{Dn}_{\mathrm{crit}}$ was quite expected from the dynamical similarity principle, but the shared Φ is a result of the fact that both modes have the same effective mass m_{eff} (see [**?**]).

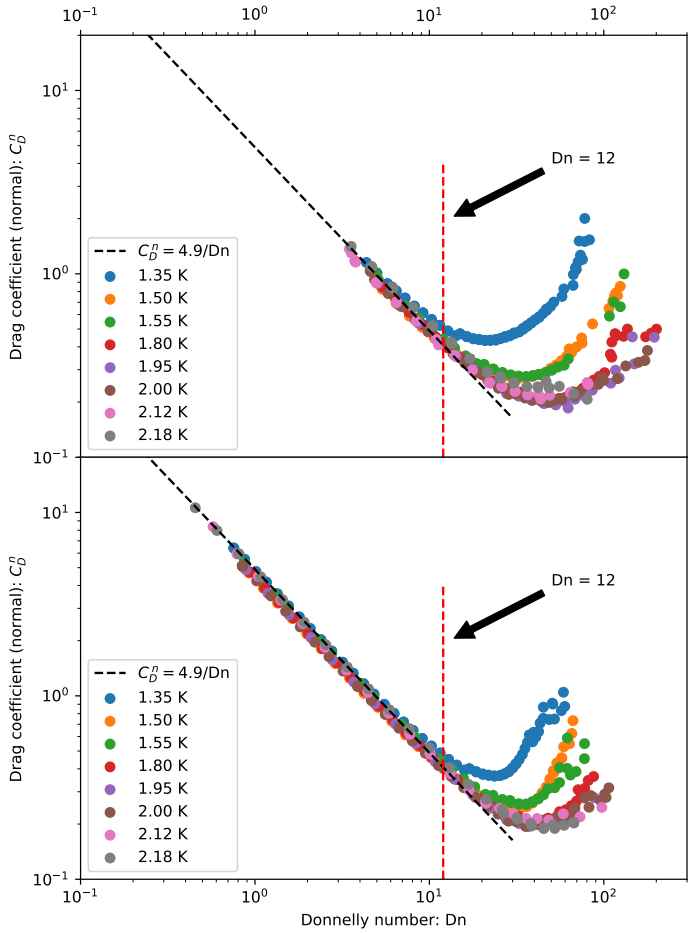

Figure 8: Normal fluid drag coefficient C_D^n as a function of the Donnelly number Dn. Top image: Measurements in fork's fundamental mode, Bottom image: Measurements in fork's overtone mode, Black dashed lines represents the laminar drag, fitted with the same pre-factor $C_D^n = 4.9/\mathrm{Dn}$ for both modes, and Red dashed lines marks the critical value of Dn, above which the onset of classical turbulence occurs.